Fault-Tolerant Control With Active Fault Diagnosis for Four-Wheel Independently Driven Electric Ground Vehicles

Rongrong Wang and Junmin Wang, *Member, IEEE*

***Abstract*—This paper presents a fault-tolerant control approach for four-wheel independently driven (4WID) electric vehicles. An adaptive control-based passive fault-tolerant controller is designed to ensure vehicle system stability and to track the desired vehicle motion when an in-wheel motor/motor driver fault happens. Due to the system actuation redundancy, it is challenging to isolate the faulty wheel and to accurately estimate the control gain of the faulty in-wheel motor/motor driver for 4WID electric vehicles. An active fault diagnosis (FD) approach is thus proposed to explicitly isolate and evaluate the fault. Based on the estimated control gain of the faulty wheel, the control efforts of all the wheels are redistributed to relieve the torque demand on the faulty wheel. Simulations using a high-fidelity CarSim full-vehicle model show the effectiveness of the proposed in-wheel motor/motor driver active fault diagnosis and fault-tolerant control approaches in various driving scenarios.**

***Index Terms*—Adaptive control, electric ground vehicle, fault diagnosis, fault tolerant, in-wheel/hub motor.**

NOMENCLATURE

a_x	Vehicle longitudinal acceleration at the center of gravity (CG).
a_y	Vehicle lateral acceleration at the CG.
C_a	Aerodynamic drag coefficient.
F_X	Effective longitudinal force acting on vehicle CG.
F_Y	Effective lateral force acting on vehicle CG.
F_{xi}	Longitudinal force of the ith tire.
F_{yi}	Lateral force of the ith tire.
F_{zi}	Normal load of the ith tire.
h_{CG}	CG height of the sprung mass.
I_z	Yaw inertia of the vehicle.
I	Wheel rotational inertia.
k_{0i}	Nominal control gain of the ith motor/motor driver.
k_i	Actual control gain of the ith motor/motor driver.
m	Vehicle sprung mass.
m_w	Total mass of the in-wheel motor, tire, and wheel.
M	Vehicle total mass.
M_Z	Effective yaw moment acting on vehicle CG.
R_{eff}	Tire effective rolling radius in meter.
s_i	Tire longitudinal slip ratio of the ith wheel.
T_i	Torque provided by the ith in-wheel motor.
u_i	Control input to the ith in-wheel motor driver.
u_l	Control signal for the left side motors.
u_r	Control signal for the right side motors.
U_0	Nominal control signal.
V_x	Vehicle longitudinal speed at mass center.
V_{rx}	Vehicle longitudinal speed reference.
V_i	Traveling velocity at the center of the ith wheel.
V_y	Vehicle lateral speed at mass center.
ω_i	Wheel rotational speed of the ith wheel.
α_i	Slip angle of the ith wheel.
σ	Front wheel steering angle.
σ_h	Hand wheel steering angle.
λ_l	Torque distribution ratio for the left side motors.
λ_r	Torque distribution ratio for the right side motors.
μ	Tire road friction coefficient (TRFC).
Ω_z	Vehicle yaw rate.
Ω_{rz}	Vehicle yaw rate reference.
Ψ_z	Vehicle yaw angle.

Manuscript received October 3, 2010; revised January 9, 2011, April 15, 2011, and June 30, 2011; accepted October 10, 2011. Date of publication October 19, 2011; date of current version December 9, 2011. This work was supported in part by the Office of Naval Research Young Investigator Program Award (Grant N00014-09-1-1018), by the Honda-OSU Partnership Program, and by the OSU Transportation Research Endowment Program. The review of this paper was coordinated by Dr. R. Langari.

The authors are with the Department of Mechanical and Aerospace Engineering, The Ohio State University, Columbus, OH 43210 USA (e-mail: wang.1862@osu.edu; wang.1381@osu.edu).

Color versions of one or more of the figures in this paper are available online at http://ieeexplore.ieee.org.

Digital Object Identifier 10.1109/TVT.2011.2172822

I. INTRODUCTION

FOUR-WHEEL independently driven (4WID) electric vehicle is a promising vehicle architecture due to its potentials in emissions and fuel consumption reductions [1]. A 4WID electric vehicle employs four in-wheel (or hub) motors to drive the four wheels, and the torque and driving/braking mode of each wheel can be controlled independently. Such an actuation flexibility together with the electric motors' fast and precise torque responses may enhance the existing vehicle control strategies, e.g., traction control system, direct yaw moment control, and other advanced vehicle motion/stability control systems [2]–[4], [6]. However, in 4WID electric vehicles, vehicle performance and stability heavily depend on the proper operations of the motors. When an in-wheel motor fault occurs, the faulty wheel may fail to provide the expected torque and thus jeopardizes the vehicle motion control performance. Without appropriate accommodations, the in-wheel motor or motor driver faults may result in an unsatisfactory performance or even instability for the 4WID electric vehicles [3], [5], [7]. Therefore, the demands on reliability, safety, and fault tolerance for 4WID electric vehicles are substantially elevated. Several

fault diagnosis (FD) and fault-tolerant control strategies for ground vehicles have been previously suggested in the literature [7]–[11]. Most of these algorithms dealt with the problems associated with conventional vehicle architectures, but not for the 4WID electric vehicles with in-wheel motors.

It is known that the 4WID electric vehicle is a typical overactuated system, and the fault diagnosis design for such systems is challenging [12], [19]. Yang *et al.* proposed a fault-tolerant path-tracking control for a 4WID electric vehicle [14], [15], but the fault diagnosis approach was not presented, and it was assumed that the fault can be identified by a certain fault diagnosis scheme. Several fault diagnosis and fault-tolerant control methods for electric motors were also proposed and reviewed in [16] and [17]. However, certain motor faults, such as the bearing fault, are difficult to diagnose with only the current and voltage sensors [17]. Almost 40–50% of all motor failures are bearing related [17], and the bearing fault is more likely to happen to an in-wheel motor due to the heavy normal load on the motor shaft and fast load changes. In addition, for some vehicle configurations, the motor current and voltage signals may not be available for higher-level vehicle control systems. Thus, the aforementioned motor/motor driver diagnosis approaches are not used here.

This paper considers the fault diagnosis and fault-tolerant control of 4WID electric vehicles using vehicle dynamics and motion signals. It is assumed that the motor control gain will reduce when a fault occurs on the motor/motor driver. An adaptive control-based passive fault-tolerant controller (FTC) is first designed to maintain vehicle stability and to track the desired vehicle motions when an in-wheel motor/motor driver fault happens. Then, an active fault diagnosis method is proposed to isolate and evaluate the fault under the designed passive FTC. Finally, the control efforts of all the in-wheel motors are readjusted based on the diagnosis result to relieve the torque demand on the faulty motor/motor driver for avoiding further actuator damages. Simulations using a high-fidelity CarSim vehicle model illustrate the effectiveness of the proposed strategy in various driving scenarios.

The rest of this paper is organized as follows. System modeling is presented in Section II. The proposed adaptive FTC is described in Section III. The active fault diagnosis method with control effort redistribution is given in Section IV. Simulation results are presented in Section V followed by conclusive remarks.

II. System Modeling

A. Vehicle Model

Ignoring the pitch and roll motions, the vehicle has three planar degrees of freedom for longitudinal motion, lateral motion, and yaw motion. A schematic of the vehicle model is shown in Fig. 1. Vehicle equations of motion in the longitudinal, lateral, and yaw directions can be expressed as

$$\begin{cases} \dot{V}_x = V_y\Omega_z - \frac{C_a}{M}V_x^2 + \frac{1}{M}F_X \\ \dot{V}_y = -V_x\Omega_z + \frac{1}{M}F_Y \\ \dot{\Omega}_z = \frac{1}{I_z}M_z \end{cases} \tag{1}$$

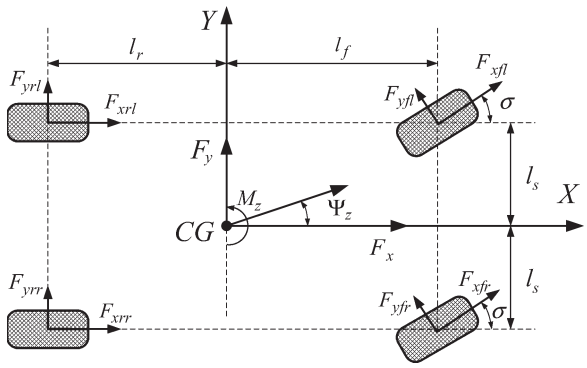

Fig. 1. Schematic of vehicle model.

where V_x and V_y are the longitudinal and lateral speeds, respectively, and Ω_z is the yaw rate. M is the mass of the vehicle, I_z is the yaw inertia, and C_a is the aerodynamic drag term. F_X, F_Y, and M_z are the total forces/moment represented by the summation of the ground forces generated at all the four tires and can be defined by

$$\begin{cases} F_X = (F_{xfl}+F_{xfr})\cos\sigma - (F_{yfl}+F_{yfr})\sin\sigma + F_{xrl} + F_{xrr} \\ F_Y = (F_{yfl}+F_{yfr})\cos\sigma + (F_{xfl}+F_{xfr})\sin\sigma + F_{yrl} + F_{yrr} \\ M_z = (F_{yfl}\sin\sigma - F_{xfl}\cos\sigma + F_{xfr}\cos\sigma - F_{yfr}\sin\sigma)l_s \\ \qquad +(F_{xrr}-F_{xrl})\,l_s - (F_{yfr}+F_{yrr})\,l_r \\ \qquad +((F_{yfr}+F_{xfl})\cos\sigma + (F_{xfr}+F_{xfl})\sin\sigma)\,l_f \end{cases} \tag{2}$$

where σ is the front wheel steering angle. Based on (2), (1) can be rewritten as

$$\begin{bmatrix} \dot{V}_x \\ \dot{V}_y \\ \dot{\Omega}_z \end{bmatrix} = \begin{bmatrix} V_y\Omega_z - \frac{C_a}{M}V_x^2 \\ -V_x\Omega_z \\ 0 \end{bmatrix} + B_yF_y + B_xF_x \tag{3}$$

where $F_x = [\,F_{xfl} \quad F_{xfr} \quad F_{xrl} \quad F_{xrr}\,]^T$ and $F_y = [\,F_{yfl} \quad F_{yfr} \quad F_{yrl} \quad F_{yrr}\,]^T$ are the tire longitudinal and lateral forces, which can be calculated by a tire model based on the measured tire slip ratios, slip angles, and normal loads. In this paper, the Magic Formula tire model [22], [24], [25] is used to calculate the tire forces. The corresponding matrices are

$$B_x = \begin{bmatrix} \frac{1}{M} & 0 & 0 \\ 0 & \frac{1}{M} & 0 \\ 0 & 0 & \frac{1}{I_z} \end{bmatrix} \times \begin{bmatrix} \cos\sigma & \cos\sigma & 1 & 1 \\ \sin\sigma & \sin\sigma & 0 & 0 \\ l_f\sin\sigma - l_s\cos\sigma & l_f\sin\sigma + l_s\cos\sigma & -l_s & l_s \end{bmatrix}$$

$$B_y = \begin{bmatrix} \frac{1}{M} & 0 & 0 \\ 0 & \frac{1}{M} & 0 \\ 0 & 0 & \frac{1}{I_z} \end{bmatrix} \times \begin{bmatrix} -\sin\sigma & -\sin\sigma & 0 & 0 \\ \cos\sigma & \cos\sigma & 1 & 1 \\ l_f\cos\sigma + l_s\sin\sigma & l_f\cos\sigma - l_s\sin\sigma & -l_r & -l_r \end{bmatrix}.$$

The mechanical motion of a motor or a vehicle is much slower than a motor's electromagnetic dynamics, implying that the dynamic response of the motor driver and in-wheel motor

can be ignored. If an in-wheel motor and its driver are treated as a unit, then the motor driver and in-wheel motor unit can be described by a control gain k_i, which is defined as

$$k_i = \frac{T_i}{u_i} \tag{4}$$

where $i \in Q := \{fl, fr, rl, rr\}$ indicates the specific wheel, T_i is the output torque of the in-wheel motor, and u_i is the torque control signal to the motor's driver. The control gain of the in-wheel motor can be obtained with experimental data [27].

The wheel rotational dynamics is represented by

$$I\dot{\omega}_i = k_i u_i - R_{\text{eff}} F_{xi} \tag{5}$$

where ω_i is the tire longitudinal rotational speed in radians per second, and R_{eff} is the tire effective rolling radius in meters. Thus, the foregoing equation can be written as

$$F_{xi} = \frac{k_i u_i - I\dot{\omega}_i}{R_{\text{eff}}}. \tag{6}$$

Therefore, one can have

$$F_x = \frac{1}{R_{\text{eff}}} \begin{bmatrix} k_{fl} & 0 & 0 & 0 \\ 0 & k_{fr} & 0 & 0 \\ 0 & 0 & k_{rl} & 0 \\ 0 & 0 & 0 & k_{rr} \end{bmatrix} \begin{bmatrix} u_{fl} \\ u_{fr} \\ u_{rl} \\ u_{rr} \end{bmatrix} - \frac{1}{R_{\text{eff}}} \begin{bmatrix} I\dot{\omega}_{fl} \\ I\dot{\omega}_{fr} \\ I\dot{\omega}_{rl} \\ I\dot{\omega}_{rr} \end{bmatrix} \tag{7}$$

where filtering needs to be applied to $\dot{\omega}_i$. Based on (7), the vehicle model (3) can be rewritten as

$$\dot{X} = f(X) + BKU \tag{8}$$

with

$$X = \begin{bmatrix} V_x \\ V_y \\ \Omega_z \end{bmatrix} \quad B = \frac{B_x}{R_{\text{eff}}}$$

$$K = \begin{bmatrix} k_{fl} & 0 & 0 & 0 \\ 0 & k_{fr} & 0 & 0 \\ 0 & 0 & k_{rl} & 0 \\ 0 & 0 & 0 & k_{rr} \end{bmatrix} \quad U = \begin{bmatrix} u_{fl} \\ u_{fr} \\ u_{rl} \\ u_{rr} \end{bmatrix}$$

$$f(X) = \begin{bmatrix} f_1(X) \\ f_2(X) \\ f_3(X) \end{bmatrix} - \begin{bmatrix} V_y\Omega_z - \frac{C_a}{M}V_x^2 \\ -V_x\Omega_z \\ 0 \end{bmatrix} + B_y F_y - \frac{B_x}{R_{\text{eff}}} \begin{bmatrix} I\dot{\omega}_{fl} \\ I\dot{\omega}_{fr} \\ I\dot{\omega}_{rl} \\ I\dot{\omega}_{rr} \end{bmatrix}.$$

B. Tire Model and Signal Calculations

In this paper, the vehicle speeds, accelerations, wheel speeds, and vehicle yaw rate are assumed to be directly measured. Global Positioning System and inertia measurement unit have been proved to be effective means of acquiring such vehicle states [24]. The tire force, slip ratio, and slip angle of each tire are calculated. The slip angle of each tire is defined as the angular difference between the orientation of a wheel and the velocity of the wheel center, i.e.,

$$\begin{cases} \alpha_{fl} = -\sigma + \tan^{-1}\left(\frac{V_y + \Omega_z l_f}{V_x - \Omega_z l_s}\right) \\ \alpha_{fr} = -\sigma + \tan^{-1}\left(\frac{V_y + \Omega_z l_f}{V_x + \Omega_z l_s}\right) \\ \alpha_{rl} = \tan^{-1}\left(\frac{V_y - \Omega_z l_f}{V_x - \Omega_z l_s}\right) \\ \alpha_{rr} = \tan^{-1}\left(\frac{V_y - \Omega_z l_f}{V_x + \Omega_z l_s}\right). \end{cases} \tag{9}$$

The tire longitudinal slip ratio is defined as the relative difference between tire circumferential speed and tire center speed, i.e.,

$$s_i = \frac{\omega_i R_{\text{eff}} - V_{xi}}{\max(V_{xi}, \omega_i R_{\text{eff}})} \tag{10}$$

with the speeds at the wheel centers being calculated by

$$\begin{cases} V_{fl} = (V_x - \Omega_z l_s)\cos\sigma + (V_y + \Omega_z l_f)\sin\sigma \\ V_{fr} = (V_x + \Omega_z l_s)\cos\sigma + (V_y + \Omega_z l_f)\sin\sigma \\ V_{rl} = V_x - \Omega_z l_s \\ V_{rr} = V_x + \Omega_z l_s. \end{cases} \tag{11}$$

The Magic Formula tire model is capable of producing characteristics that can closely match with the measured curves for the tire lateral force F_{yi}, longitudinal force F_{xi}, and aligning moment as functions of slip angle α_i and longitudinal slip ratio s_i [22], [23], [30]. The basic equations are

$$\begin{cases} y(h) = Z\sin\left\{W\tan^{-1}\left[B_t x - E(Bx - \tan^{-1}B_t h)\right]\right\} \\ Y(H) = y(h) + S_v \\ h = X + S_h \end{cases} \tag{12}$$

where $Y(X)$ represents the tire longitudinal force, lateral force, or self-aligning moment, and h is tire slip or slip angle. The coefficient B_t is the stiffness factor, W is the shape factor, Z is the peak factor, and E is the curvature factor. S_h and S_v denote the horizontal and vertical shifts, respectively. These coefficients in the model are tuned to fit experimental data for a given tire on a test patch. A similar form can be used to represent the case of combined slip and slip angle [23].

As the vehicle parameters are assumed to be known, the tire normal loads can be calculated as

$$\begin{cases} F_{zfl} = m_w g + \frac{mgl_r}{2(l_r+l_f)} - \frac{mh_{\text{CG}}a_x}{2(l_r+l_f)} - \frac{mh_{\text{CG}}a_y}{4l_s} \\ F_{zfr} = m_w g + \frac{mgl_r}{2(l_r+l_f)} - \frac{mh_{\text{CG}}a_x}{2(l_r+l_f)} + \frac{mh_{\text{CG}}a_y}{4l_s} \\ F_{zrl} = m_w g + \frac{mgl_f}{2(l_r+l_f)} + \frac{mh_{\text{CG}}a_x}{2(l_r+l_f)} - \frac{mh_{\text{CG}}a_y}{4l_s} \\ F_{zrr} = m_w g + \frac{mgl_f}{2(l_r+l_f)} + \frac{mh_{\text{CG}}a_x}{2(l_r+l_f)} + \frac{mh_{\text{CG}}a_y}{4l_s} \end{cases} \tag{13}$$

where h_{CG} is the height of the sprung mass CG, and m_w is the total mass of tire, in-wheel motor, and wheel.

III. Passive FTC Design

Some common motor faults, such as the fault in either a motor winding or an inverter phase, can be modeled as the

reduction in the motor control gain. In this paper, it is assumed that when a fault happens in an in-wheel motor/motor driver, the respective motor control gain will jump to a lower constant value. In addition, we assume that only one of the four in-wheel motors has a fault. An FTC is designed in this section to maintain the vehicle stability and desired performance even when a fault happens. The control objective is to make the faulty vehicle motion control performance the same as that of the healthy one, which requires the faulty vehicle can still follow the longitudinal speed and yaw rate references. The vehicle lateral speed is not considered in this paper, and the model for controller design can be written as follows based on (3):

$$\begin{bmatrix} \dot{V}_x \\ \dot{\Omega}_z \end{bmatrix} = \begin{bmatrix} f_1(X) \\ f_3(X) \end{bmatrix} + \frac{1}{R_{\text{eff}}} \begin{bmatrix} \frac{\cos\sigma}{M} & \frac{\cos\sigma}{M} & \frac{1}{M} & \frac{1}{M} \\ \frac{l_f \sin\sigma - l_s \cos\sigma}{I_z} & \frac{l_f \sin\sigma + l_s \cos\sigma}{I_z} & \frac{-l_s}{I_z} & \frac{l_s}{I_z} \end{bmatrix} KU. \quad (14)$$

We can see from (14) that the two control efforts on the same side of the vehicle have similar effects on the vehicle longitudinal speed and yaw rate. When the vehicle is under healthy condition, one has $k_{fl} = k_{fr} = k_{rl} = k_{rr} = k_0$, with k_0 being the nominal control gain of the healthy motor. Therefore, based on (4), one has

$$\begin{cases} \lambda_l = \frac{u_{fl}}{u_{rl}} \\ \lambda_r = \frac{u_{fr}}{u_{rr}} \end{cases} \quad (15)$$

where λ_l and λ_r are the ratios of the front wheel torque to the rear wheel torque on the left and right sides of the vehicle, respectively. Denoting

$$\begin{cases} u_l = u_{rl} \\ u_r = u_{rr} \end{cases} \quad (16)$$

the vehicle model (14) can further be written as

$$\begin{bmatrix} \dot{V}_x \\ \dot{\Omega}_z \end{bmatrix} = \begin{bmatrix} f_1(X) \\ f_3(X) \end{bmatrix} + \frac{1}{R_{\text{eff}}} \begin{bmatrix} \frac{1}{M} & 0 \\ 0 & \frac{l_s}{I_z} \end{bmatrix} \begin{bmatrix} k_{lx} & k_{rx} \\ -k_{lz} & k_{rz} \end{bmatrix} \begin{bmatrix} u_l \\ u_r \end{bmatrix} \quad (17)$$

with

$$\begin{cases} k_{lx} = \lambda_l k_{fl} \cos\sigma + k_{rl} \\ k_{rx} = \lambda_r k_{fr} \cos\sigma + k_{rr} \\ k_{lz} = \lambda_l k_{fl} \cos\sigma + k_{rl} - \lambda_l k_{fl} \frac{l_f \sin\sigma}{l_s} \\ k_{rz} = \lambda_r k_{fr} \cos\sigma + k_{rr} + \lambda_r k_{fr} \frac{l_f \sin\sigma}{l_s}. \end{cases} \quad (18)$$

In this paper, the four motors are assumed to be identical; thus, we take both of the torque distribution ratios $\lambda_{l,r}$ as one. Note that λ_l and λ_r may be adjusted. As both λ_l and λ_r are known, the change of λ_l and λ_r will not affect the FTC design, which will be shown in the following part of this section. When a fault happens, the actual value of k_j with $j \in \{lx\ rx\ lz\ rz\}$ will be unknown as the control gain of the faulty motor is undetermined. By ignoring the σ variation, k_j is assumed to be piecewise constant. Here, an adaptive controller, which does not need the accurate value of k_j, is designed as the passive FTC for stabilizing the faulty vehicle and tracking the desired vehicle motions. Define the Lyapunov function candidate as

$$V = \frac{1}{2}\left((k_{lx} - \hat{k}_{lx})^2 + (k_{rx} - \hat{k}_{rx})^2 + (k_{lz} - \hat{k}_{lz})^2 + (k_{rz} - \hat{k}_{rz})^2\right) + \frac{1}{2}\left(e_{rx}^2 + e_{\Omega}^2\right) \quad (19)$$

where $\hat{k}_j$ is the estimation of k_j, $e_{rx} = V_{rx} - V_x$, and $e_{\Omega} = \Omega_{rz} - \Omega_z$, with V_{rx} and Ω_{rz} being the longitudinal speed and yaw rate references. The time derivative of V is

$$\begin{aligned} \dot{V} =& e_{rx}\left(\dot{V}_{rx} - f_1(X) - \frac{k_{lx}u_l + k_{rx}u_r}{MR_{\text{eff}}}\right) \\ &+ e_{\Omega}\left(\dot{\Omega}_{rz} - f_3(X) - \frac{-l_s k_{lz}u_l + l_s k_{rz}u_r}{I_Z R_{\text{eff}}}\right) \\ &- \left(k_{lx} - \hat{k}_{lx}\right)\dot{\hat{k}}_{lx} - \left(k_{rx} - \hat{k}_{rx}\right)\dot{\hat{k}}_{rx} - \left(k_{lz} - \hat{k}_{lz}\right)\dot{\hat{k}}_{lz} \\ &- \left(k_{rz} - \hat{k}_{rz}\right)\dot{\hat{k}}_{rz} \\ =& e_{rx}\left(\dot{V}_{rx} - f_1(X)\right) + e_{\Omega}\left(\dot{\Omega}_{rz} - f_3(X)\right) \\ &- \left(\frac{e_{rx}k_{lx}u_l}{MR_{\text{eff}}} + k_{lx}\dot{\hat{k}}_{lx}\right) \\ &- \left(\frac{e_{rx}k_{rx}u_r}{MR_{\text{eff}}} + k_{rx}\dot{\hat{k}}_{rx}\right) + \left(\frac{e_{\Omega}l_s k_{lz}u_l}{I_Z R_{\text{eff}}} - k_{lz}\dot{\hat{k}}_{lz}\right) \\ &- \left(\frac{e_{\Omega}l_s k_{rz}u_r}{I_Z R_{\text{eff}}} + k_{rz}\dot{\hat{k}}_{rz}\right) \\ &+ \hat{k}_{lx}\dot{\hat{k}}_{lx} + \hat{k}_{rx}\dot{\hat{k}}_{rx} + \hat{k}_{lz}\dot{\hat{k}}_{lz} + \hat{k}_{rz}\dot{\hat{k}}_{rz}. \end{aligned} \quad (20)$$

By selecting

$$\begin{cases} \dot{\hat{k}}_{lx} = -\frac{e_{rx}u_l}{MR_{\text{eff}}} \\ \dot{\hat{k}}_{rx} = -\frac{e_{rx}u_r}{MR_{\text{eff}}} \\ \dot{\hat{k}}_{lz} = \frac{e_{\Omega}l_s u_l}{I_Z R_{\text{eff}}} \\ \dot{\hat{k}}_{rz} = \frac{e_{\Omega}l_s u_r}{I_Z R_{\text{eff}}} \end{cases} \quad (21)$$

one can rewrite $\dot{V}$ as

$$\begin{aligned} \dot{V} =& e_{rx}\left(\dot{V}_{rx} - f_1(X)\right) + e_{\Omega}\left(\dot{\Omega}_{rz} - f_3(X)\right) \\ &- \frac{e_{rx}\hat{k}_{lx}u_l + e_{rx}\hat{k}_{rx}u_r}{MR_{\text{eff}}} + \frac{e_{\Omega}l_s\hat{k}_{lz}u_l - e_{\Omega}l_s\hat{k}_{rz}u_r}{I_Z R_{\text{eff}}}. \end{aligned} \quad (22)$$

If the control laws for u_r and u_l can be chosen such that

$$\begin{cases} L_1 e_{rx}^2 + e_{rx}\left(\dot{V}_{rx} - f_1(X)\right) = \frac{e_{rx}}{MR_{\text{eff}}}\left(\hat{k}_{lx}u_l + \hat{k}_{rx}u_r\right) \\ L_2 e_{\Omega}^2 + e_{\Omega}\left(\dot{\Omega}_{rz} - f_3(X)\right) = \frac{e_{\Omega}l_s}{I_Z R_{\text{eff}}}\left(-\hat{k}_{lz}u_l + \hat{k}_{rz}u_r\right) \end{cases} \quad (23)$$

with $L_1, L_2 > 0$, then one has

$$\dot{V} = -L_1 e_{rx}^2 - L_2 e_{\Omega}^2 < 0. \quad (24)$$

By Barbalat's lemma, it can be concluded that both e_{rx} and e_Ω will converge to zero [20], [26], which means that the actual longitudinal speed and yaw rate will asymptotically follow the references.

Based on (23), the control law can be written as

$$\begin{cases} u_l = \dfrac{R_{\text{eff}}\left(M\hat{k}_{lz}\left(L_1 e_{rx}+\dot{V}_{rx}-f_1(X)\right)\right)-\frac{I_z}{l_s}\hat{k}_{lx}\left(L_2 e_\Omega+\dot{\Omega}_{rz}-f_3(X)\right)}{\hat{k}_{lx}\hat{k}_{rz}+\hat{k}_{rx}\hat{k}_{lz}} \\ u_r = \dfrac{R_{\text{eff}}\left(M\hat{k}_{lz}\left(L_1 e_{rx}+\dot{V}_{rx}-f_1(X)\right)\right)+\frac{I_z}{l_s}\hat{k}_{lx}\left(L_2 e_\Omega+\dot{\Omega}_{rz}-f_3(X)\right)}{\hat{k}_{lx}\hat{k}_{rz}+\hat{k}_{rx}\hat{k}_{lz}} \end{cases}. \tag{25}$$

The actual motor control signal vector U to the motors can be calculated as

$$U = \begin{bmatrix} u_{fl} \\ u_{fr} \\ u_{rl} \\ u_{rr} \end{bmatrix} = \begin{bmatrix} \lambda_l u_l \\ \lambda_r u_r \\ u_l \\ u_r \end{bmatrix}. \tag{26}$$

To guarantee that the control signals are bounded, a projection method is used to modify the update law (21) by projecting the gradient of the parameters onto the supporting plane when the estimated parameters are on the boundary and moving outside of the boundary [21]. As the faulty motor control gain is unknown before diagnosis, and the faulty wheel control gain is assumed to be smaller than the nominal value, the upper bound of the faulty motor control gain should still be the upper bound of the healthy motor's control gain. As $\lambda_{l,r}$ are assumed to be 1 in this study, based on the control gain definition (18), one can see that $\hat{k}_j$ satisfies

$$\begin{cases} 0 < \varepsilon_1 < \hat{k}_{lx} \le 2k_{\max} \\ 0 < \varepsilon_1 < \hat{k}_{rx} \le 2k_{\max} \\ 0 < \varepsilon_2 < \hat{k}_{lz} < (q+1)\,k_{\max} \\ 0 < \varepsilon_2 < \hat{k}_{rz} < (q+1)\,k_{\max} \end{cases} \tag{27}$$

where $q = \sqrt{l_s^2 + l_f^2}/l_s$, ε_1 and ε_2 are small positive constants, and $k_{\max}$ is the maximal control gain of a single motor. For the case of straight-line driving, if only one motor is in fault, both ε_1 and ε_2 will be equal to the single motor's minimal control gain $k_{\min}$. Based on the projection method, the update law for $\hat{k}_{lx}$ in (21) can be modified as

$$\dot{\hat{k}}_{lx} = \begin{cases} p & \text{if } (0 < \varepsilon_1 < \hat{k}_{lx} \le 2k_{\max}) \\ & \text{or } (\hat{k}_{lx} = \varepsilon_1 \quad \text{and} \quad p > 0) \\ & \text{or } (\hat{k}_{lx} = 2k_{\max} \quad \text{and} \quad p < 0) \\ 0 & \text{otherwise} \end{cases} \tag{28}$$

where p is defined as $p = -(e_{rx}u_l/R_{\text{eff}}M)$. The update law for $\hat{k}_{rx}$, $\hat{k}_{lz}$, and $\hat{k}_{rz}$ can be modified in a similar fashion.

IV. Active Fault Diagnosis Design and Control Effort Redistribution

The preceding passive FTC can ensure vehicle control stability even when a motor fault occurs. However, the faulty wheel still needs to provide torque, whose magnitude may not correlate with the health status of the faulty motor/motor driver. Such a situation is undesirable because excessive usage of the faulty wheel motor/motor driver may further deteriorate the fault and induce additional damage to the actuator. It is better to actively adjust the use of the faulty motor according to its reduced control gain. Based on (14), one can see that the two control efforts on the same vehicle side have very close effects on the vehicle longitudinal speed and yaw rate dynamics, and the control effects will be the same if the vehicle runs in a straight line. In this section, an active fault diagnosis method is proposed to explicitly locate the faulty motor on the faulty side and to estimate the changed control gain for a better reallocation of the total control effort.

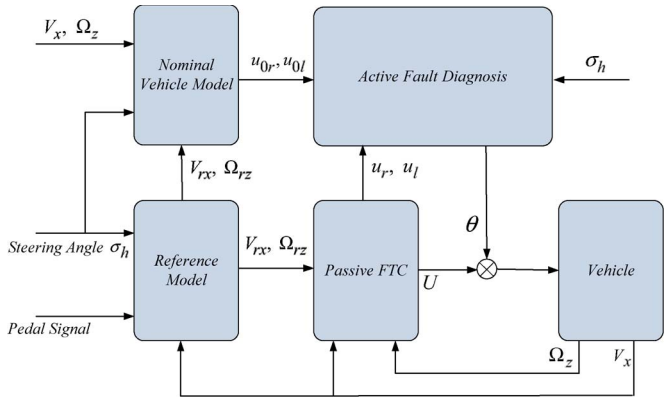

Fig. 2. Block diagram of the proposed control system with active fault diagnosis.

A block diagram of the proposed control system is shown in Fig. 2. Note that both the vehicle speed reference V_{rx} and the yaw rate reference Ω_{rz} can be generated from the driver's steering angle, accelerator/brake pedal signals, and vehicle states through reference models. The reference model for the longitudinal speed can be written as

$$V_{rx} = V_0 + \int_{t_0}^{t} a_{rx}\,dt \tag{29}$$

where V_0 is the initial vehicle speed at time t_0, and a_{rx} is the desired vehicle acceleration which can be calculated from the pedal position. The yaw rate reference is a function of the driver's steering wheel angle and vehicle speed and can be written as [28]

$$\Omega_{rz} = \frac{\hat{V}_x}{(\tau_1 s+1)(\tau_2 s+1)}\sigma_h \tag{30}$$

where $\hat{V}_x = GR \cdot k_a \cdot V_x/((k_b V_x^2+1)\cdot l)$, τ_1 and τ_2 are time constants, l is the vehicle wheel base, k_a is the gain of the reference model, k_b is the stability factor, and GR is the gear ratio of the steering mechanism linkage.

Based on the measured vehicle yaw rate and longitudinal speed, the passive FTC ensures the stability of the vehicle and tracks the desired motions. The active fault diagnosis block first determines which vehicle side has a faulty wheel and then estimates the motor control gains on the corresponding side with the assistance from the additional gain multipliers. This way, the faulty wheel is located, and the faulty wheel control gain can also be estimated. Note that the passive FTC ascertains the stability and tracking performance of the vehicle even if a fault happens or the motor control gain is changed by the active fault diagnosis approach.

Suppose that the passive FTC, using the nominal vehicle model (without faults), can give a nominal control signal $U_0 = [u_{0l}\ u_{0l}]^T$ that can maintain the motion of a reference (healthy) vehicle model as desired. After the FTC stabilizes the motions of the faulty vehicle, the following holds:

$$\begin{cases} u_r k_{rx} + u_l k_{lx} = u_{0r} k_{0rx} + u_{0l} k_{0lx} \\ u_r k_{rz} - u_l k_{lz} = u_{0r} k_{0rz} - u_{0l} k_{0lz}. \end{cases} \tag{31}$$

Note that $u_{0r}k_{0rx} + u_{0l}k_{0lx}$ represents the desired total torque from the four in-wheel motors, and this total torque controls the vehicle longitudinal speed. $u_{0r}k_{0rz} - u_{0l}k_{0lz}$ is the desired torque difference between the right and left sides of the vehicle, and it will compensate the vehicle yaw rate tracking error.

When a motor fault happens, the following holds based on (31):

$$\begin{bmatrix} u_r \\ u_l \end{bmatrix} = \begin{bmatrix} k_{rx} & k_{lx} \\ k_{rz} & -k_{lz} \end{bmatrix}^{-1} \begin{bmatrix} k_{0rx} & k_{0lx} \\ k_{0rz} & -k_{0lz} \end{bmatrix} \begin{bmatrix} u_{0r} \\ u_{0l} \end{bmatrix}. \tag{32}$$

Supposing that the left side has a faulty motor, then

$$\begin{aligned} \begin{bmatrix} u_r \\ u_l \end{bmatrix} &= \frac{\begin{bmatrix} -k_{lz} & -k_{lx} \\ -k_{0rz} & k_{0rx} \end{bmatrix} \begin{bmatrix} k_{0rx} & k_{0lx} \\ k_{0rz} & -k_{0lz} \end{bmatrix} \begin{bmatrix} u_{0r} \\ u_{0l} \end{bmatrix}}{-k_{0rx}k_{lz} - k_{lx}k_{0rz}} \\ &= \begin{bmatrix} u_{0r} \\ u_{0l} \end{bmatrix} + \frac{u_{0l} \begin{bmatrix} k_{0lx}k_{lz} - k_{0lz}k_{lx} \\ k_{0rx}(k_{0lz} - k_{lz}) + k_{0rz}(k_{0lx} - k_{lx}) \end{bmatrix}}{k_{0rx}k_{lz} + k_{lx}k_{0rz}}. \end{aligned} \tag{33}$$

Based on the definition of k_j, $j \in \{lx\ rx\ lz\ rz\}$ in (18), after some calculations, one can find $|k_{0lx}k_{lz} - k_{0lz}k_{lx}| < |k_{0rx}(k_{0lz} - k_{lz}) + k_{0rz}(k_{0lx} - k_{lx})|$, which means that if the left side has a faulty motor, then the following holds:

$$|u_r - u_{0r}| < |u_l - u_{0l}|. \tag{34}$$

Similarly, if the right side has a faulty motor, then one has

$$|u_r - u_{0r}| > |u_l - u_{0l}|. \tag{35}$$

If no fault happens, then $|u_r - u_{0r}| = |u_l - u_{0l}|$. In practice, a threshold $|u_j - u_{0j}| \geq \Delta u > 0$ may need to be applied to avoid false alarms.

In addition, suppose that the left side is found to have a faulty wheel. Then, (31) can be rewritten as

$$\begin{cases} u_r k_{0rx} + u_l k_{lx} = u_{0r} k_{0rx} + u_{0l} k_{0lx} \\ u_r k_{0rz} - u_l k_{lz} = u_{0r} k_{0rz} - u_{0l} k_{0lz} \end{cases} \tag{36}$$

which means

$$\begin{aligned} u_r(k_{0rx} - k_{0rz}) + u_l(k_{lx} + k_{lz}) \\ = u_{0r}(k_{0rx} - k_{0rz}) + u_{0l}(k_{0lx} + k_{0lz}). \end{aligned} \tag{37}$$

Based on (18), one has

$$\left(\cos\sigma - \frac{l_f \sin\sigma}{2l_s}\right) \lambda_l k_{fl} + k_{rl} = z \tag{38}$$

with

$$z = \frac{-\frac{(u_{0r} - u_r) l_f \sin\sigma}{2l_s} + u_{0l}\left(\left(\cos\sigma + \frac{l_f \sin\sigma}{2l_s}\right)\lambda_r k_{0fr} + k_{0rr}\right)}{u_l}. \tag{39}$$

In (38), for k_{fl} and k_{rl}, one (the faulty one) of them is less than the nominal value, and the other (healthy one) is the nominal motor control gain value. The faulty wheel and its control gain may not be well determined from (38) alone. It is known that, based on (4), the motor control gain can equivalently be changed by multiplying a positive value to its respective control signal dictated by the fault-tolerant control law. Such additional motor control gain multipliers, i.e., θ_1, $\theta_2 \leq 1$, can be piecewise constants. After the introduction of such multipliers, we have

$$\left(\cos\sigma - \frac{l_f \sin\sigma}{2l_s}\right) \theta_1 \lambda_l k_{fl} + \theta_2 k_{rl} = z' \tag{40}$$

where z' can be calculated by (39) with the control signals after the additional motor control gain multipliers are introduced. Based on (40), one can readily formulate a standard parameter estimation scheme as

$$\left[\left(\cos\sigma - \frac{l_f \sin\sigma}{2l_s}\right) \lambda_l k_{fl} \quad k_{rl}\right] [\theta_1 \quad \theta_2]^T = z' \tag{41}$$

with $\theta = [\theta_1, \theta_2]^T$ being the regressor vector whose elements can be artificially adjusted, within a certain range, to ensure the persistence of excitation condition and thus the reliable estimations for k_{fl} and k_{rl} [26]. Parameter estimation algorithms, such as the recursive least-square estimator, can be utilized to estimate the control gains. Note that the passive FTC designed in the previous section can still make the vehicle follow the references even when additional piecewise constant gain multipliers are introduced. This is because the piecewise constant gain multipliers essentially make the motor control gains jump to new constant values, and such a motor control gain change can be accommodated by the adaptive control law. In addition, note that the control signals between the occurrence of a fault and the introduction of gain multipliers will be used in the active fault diagnosis to estimate the faulty wheel control gain. Therefore, this additional gain multiplier should be introduced only after the passive FTC renders all the vehicle states to the references, i.e., if the tracking errors converge to zero, then the active fault diagnosis phase can be initiated. If the fault happens on the right side of the vehicle, the faulty wheel control gain can be estimated in a similar way.

Based on the fault diagnosis and the control gain estimation results, the use of a faulty motor should be discouraged. Consider the cost function for the two wheels on the faulty side

$$J_f = w_0 u_h^2 + w_f u_f^2 \tag{42}$$

where u_h and u_f represent the control signals for the healthy and faulty motors on the faulty side of the vehicle, respectively. One possible weighting factor for the faulty wheel can be

$$w_f = \eta w_0 \tag{43}$$

TABLE I
PARAMETERS OF THE VEHICLE MODEL IN CARSIM

Parameters	Values
M	880 kg
m	700kg
m_w	45kg
I	3 kg*m^2
R_{eff}	0.33 m
l_s	0.7m
l_f	0.8m
l_r	0.8m
C_a	0.5
I_z	447.6 kg*m^2

where $\eta = k_0/k_{if}$, and k_{if} is the estimated control gain for the faulty wheel. The cost function can be minimized if u_h and u_f satisfy

$$\frac{u_h}{u_f} = \eta \frac{w_f}{w_0} = \eta^2. \tag{44}$$

It can be seen that the weighting factors do not change when there is no fault. However, if there is a fault, the control gain of the faulty wheel decreases, and w_f will increase. If the fault is large, then the associated component is more heavily weighted. The weighting factor $w_f \to \infty$ if the actual control gain of the faulty wheel goes to 0, which means that the use of the faulty wheel will be strongly discouraged. Equation (44) also means that the torque distribution ratio λ_l or λ_r defined in (15) will be adjusted based on the fault estimation result. Note that the vehicle stability can still be maintained by the FTC after the torque distribution ratio changes. In addition, note that other torque redistribution methods can be adapted as well, for example, the faulty wheel can be completely turned off, and this means the torque distribution ratio on the faulty side will be 1 or 0, depending on whether the front or rear in-wheel motor has a fault.

V. SIMULATION STUDIES

Three simulation cases based on a high-fidelity full-vehicle model constructed in CarSim were conducted. The vehicle parameters in the simulations are listed in Table I. These parameters are taken from an actual prototype 4WID electric vehicle with in-wheel motors developed in the authors' group at The Ohio State University [27].

A. J-Turn Simulation

In this simulation, the nominal control gain of each motor was set to 30, and a fault, with reduced control gain of 15, was introduced to the rear-right motor after 2 s. The vehicle initial speed was 10 km/h, and the TRFC was set as 0.4. A counterclockwise turn was introduced with the front wheel steering angle shown in Fig. 3. At 2.3 s, the passive FTC stabilized the vehicle, and the gain multiplier was introduced at this time to the front-right and rear-right motors by multiplying the control signals with $\theta_1 = 0.5$ and $\theta_1 = 1.0$, respectively. It

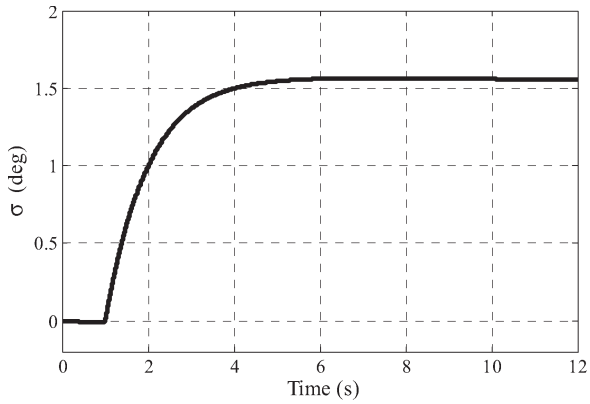

Fig. 3. Front wheel steering angle in the J-turn simulation.

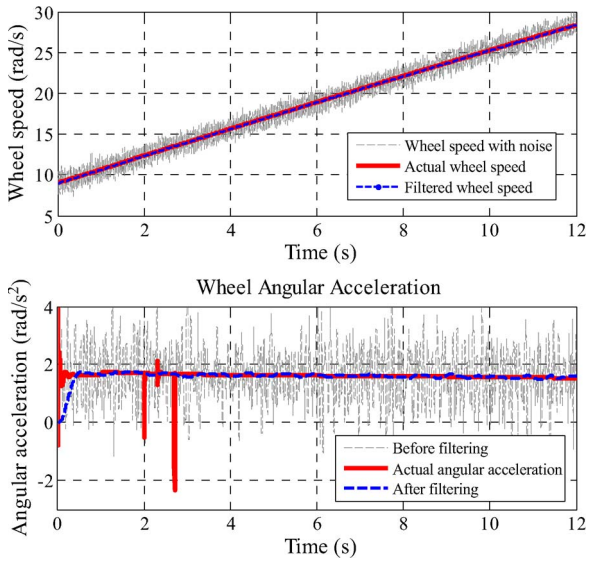

Fig. 4. Wheel speed and wheel angular acceleration estimation results.

should be noted that other combinations of $[\theta_1\ \theta_1]^T$ can be used as well.

The wheel angular acceleration was obtained by taking the time derivative of the wheel speed signal. As actual measurement may contain noises, it is not suitable to directly differentiate the wheel speed signal. Thus, the wheel speed is first filtered with a low-pass filter before being differentiated. To better show the effectiveness of the method, a white noise was added to the wheel speed signal in the simulation. The wheel speed and its angular acceleration estimation results are displayed in Fig. 4. Note that an additional low-pass filter was used to further reduce the noise of the angular acceleration from the time derivative of the filtered wheel speed. One can see from this figure that the proposed method can give good wheel angular acceleration. The actual wheel speed and the actual angular acceleration signals in the figure were directly generated from the CarSim model. Note that the glitches on the actual angular acceleration were caused by wheel torque sudden changes. Other methods of estimating wheel angular acceleration can be found in the literature, such as [29].

The torque values provided by all the four motors are shown in Fig. 5, which indicates that the two wheels on the healthy side (left side) always provide very similar torques no matter

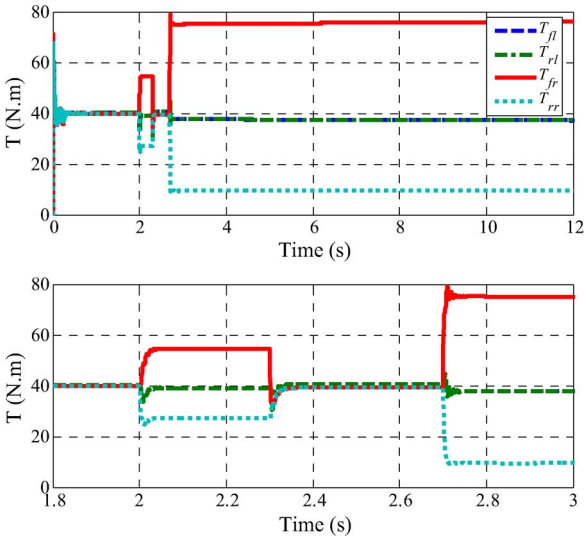

Fig. 5. Motor torques in the J-turn simulation (FTC with active fault diagnosis).

whether there was a fault or not on the other two wheels. After 2 s, the healthy motor on the faulty vehicle side increased the torque because the passive FTC increased the control signal to the faulty side to compensate motor fault. At 2.3 s, the FTC has stabilized the vehicle, and the additional gain multiplier was introduced to the two motors on the fault side. We can see that the two motors on the faulty side started to provide the same torque level due to the selection of the gain multipliers. At 2.7 s, the active diagnosis period finished as the estimated control gain converged, and the healthy motor (front right) on the faulty side began to provide most of the torque required for this side as the control efforts were redistributed according to the change of the weighting factors in the cost function. Meanwhile, the torque provided by the faulty wheel (rear right) was significantly reduced with the intention of avoiding further damage on this actuator.

The control gain estimations for the wheels on the faulty side, where the active FD was applied, are shown in Fig. 6. We can see that the estimated control gain of the faulty wheel is very close to the actual value, which changed from 30 to 15 at 2 s due to the fault, whereas the estimated control gain for the healthy wheel converges to the nominal value. Note from Fig. 6 that there are small steady state estimation errors. This may be attributed to the unmodeled dynamics in the system. However, one can still conclude that the proposed method can give very good control gain estimations. Based on the estimated faulty wheel control gain, the weight for the fault wheel in the cost function is readjusted to better allocate the control effort and to discourage the use of the faulty wheel, as shown in Fig. 5.

Fig. 7 displays the vehicle longitudinal velocity and yaw rate under the proposed fault diagnosis and FTC. The vehicle global trajectories are compared in Fig. 8. To better show the effectiveness of the proposed controller, the performance of an uncontrolled vehicle with the same fault was also compared. As Fig. 7 indicates, the controlled vehicle can follow the reference velocity and yaw rate well, whereas the uncontrolled vehicle failed to follow the references as the faulty wheel failed to provide the required torque. The failure on tracking the vehicle

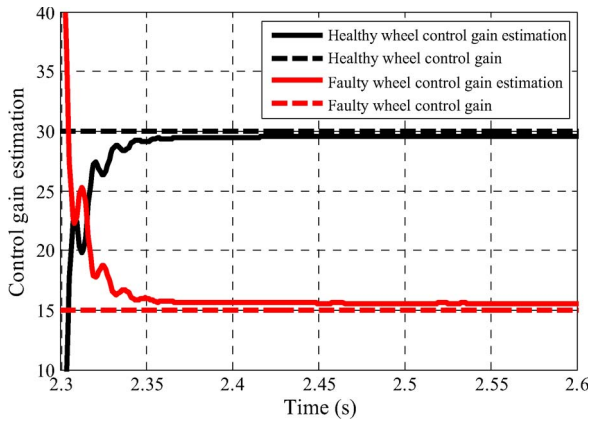

Fig. 6. Control gain estimations on the faulty side in the J-turn simulation.

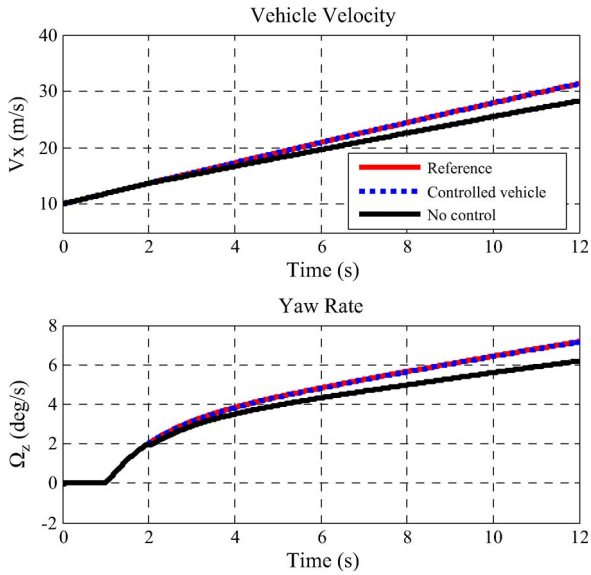

Fig. 7. Longitudinal velocities and yaw rates in the J-turn simulation.

motion references also induced the deviation of the vehicle trajectory, as shown in Fig. 8. We can see from Fig. 8 that the control results by the FTCs with and without active fault diagnosis are very close to each other; this is because that the passive FTC ensured the vehicle tracking performance no matter whether the proposed active fault diagnosis is used or not. Note that one of the main advantages of using the active diagnosis method is that the control effort of each in-wheel motor can be reallocated based on the estimated fault grade.

B. Single-Lane Change during Acceleration

In this simulation, the desired vehicle speed was accelerated from 50 to 60 km/h in 10 s. The TRFC was chosen as 0.8. The front wheel steering angle change is shown in Fig. 9. At 2 s, a complete motor fault was introduced to the rear-right motor, which made the control gain decrease to 0.

The motor torque values are shown in Fig. 10. The fault was introduced at 2 s, and at 2.3 s, the torque stopped changing, and at this time, the gain multipliers in active fault diagnosis were introduced to faulty side wheels by multiplying the control signals of the front-right and rear-right wheels with $\theta_1 = 1.0$

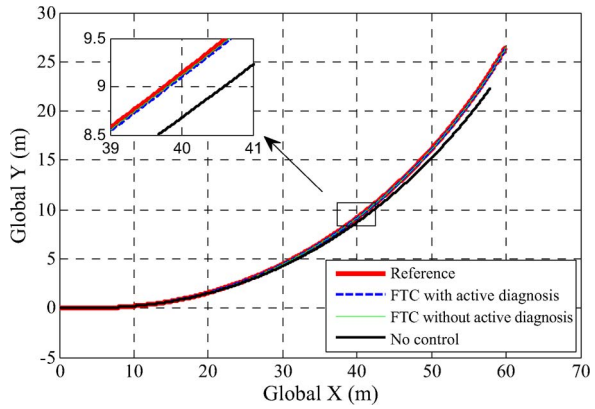

Fig. 8. Vehicle trajectories in the J-turn simulation.

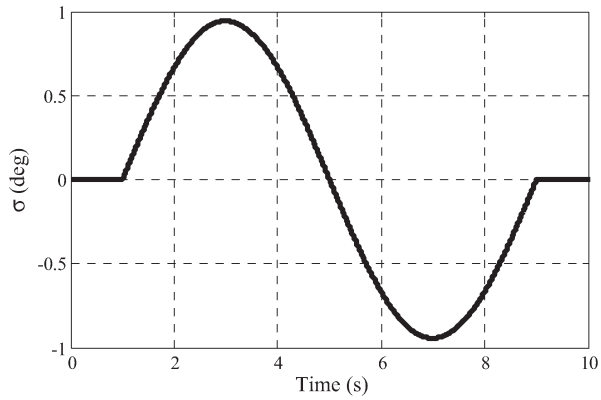

Fig. 9. Front wheel steering angle in the single-lane change simulation.

and $\theta_1 = 0.5$, respectively. We can see from Fig. 10 that the torques do not have the transient response at 2.3 s, which is different from that shown in Fig. 5. This is because that the control signal to the faulty wheel is changed, and this control signal change will not affect the vehicle states as the fault wheel control gain is zero in this case. Fig. 11 shows the control gain estimations for the faulty side two wheels. We can observe that the active fault diagnosis can also give very good control gain estimation in this case. Note that there is no transient process in the control gain estimation in this case because the faulty wheel control gain decreased to zero due to the fault (total fault), and thus, the control gain multipliers to the fault in-wheel motor do not have any effect on the vehicle motion.

The vehicle longitudinal velocity and yaw rate controlled by the FTC with active diagnosis are shown in Fig. 12, which indicates again that the controlled vehicle can follow the reference velocity and yaw rate well, whereas the uncontrolled vehicle failed to do so as long as the fault was introduced. The vehicle global trajectories are compared in Fig. 13, which displays that both trajectories given by the FTC with and without the active diagnosis can follow the reference trajectory well.

C. Acceleration on a Split-μ Surface

The foregoing two simulations were performed on surfaces with uniform frictional condition, and the vehicle was turning. In this simulation, a split-μ road was used, and the steering angle was set as zero. The desired vehicle speed was accelerated

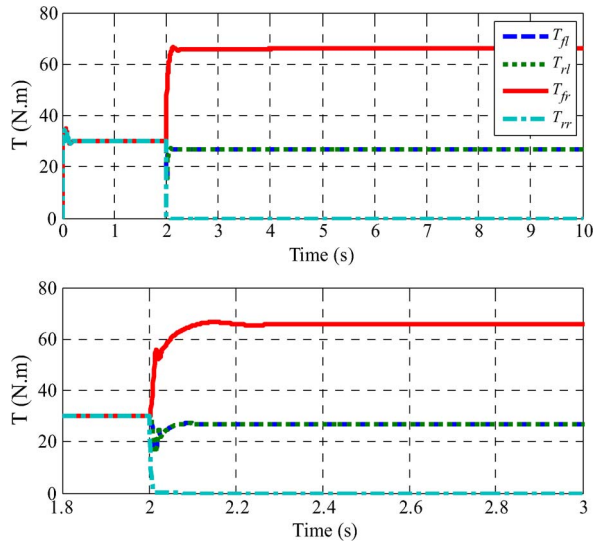

Fig. 10. Motor torques in the single lane change (FTC with active fault diagnosis).

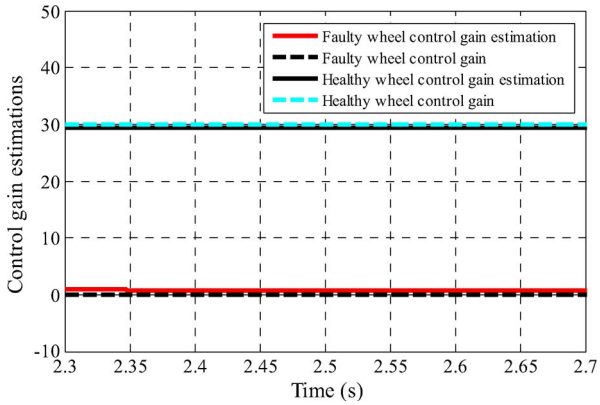

Fig. 11. Control gain estimations of the two wheels on the faulty side in the single-lane change simulation.

from 30 to 55 km/h in 12 s. The tire-road friction coefficient on the left side of the road was set as 0.2, and the right side was chosen as 0.7. The nominal control gain of each motor is set to 40, and a fault that reduced the control gain to 0.3 times of the nominal value was introduced to the rear-right motor after 2 s. The additional gain multipliers introduced the front-right motor and rear-right wheel were $\theta_1 = 1.0$ and $\theta_1 = 0.5$, respectively.

The motor torque values are shown in Fig. 14. It can be seen that the torque from the fault wheel decreased at 2.3 s; this is because that the faulty motor control gain was decreased by 0.5 by the multiplier. The control gain estimations of the faulty side two motors are shown in Fig. 15, which illustrates again that the estimation results are good. At 2.7 s, the faulty wheel torque decreased again; this is because that the four-wheel control efforts were redistributed with the control gain estimation results, and the faulty wheel was assigned to a smaller desired torque.

Fig. 16 shows the longitudinal velocity and yaw rate in this split-μ simulation. It can be seen again that the controlled vehicle can follow the references very well. The vehicle global trajectories are compared in Fig. 17. One can observe that both the FTC with and without active fault diagnosis can control

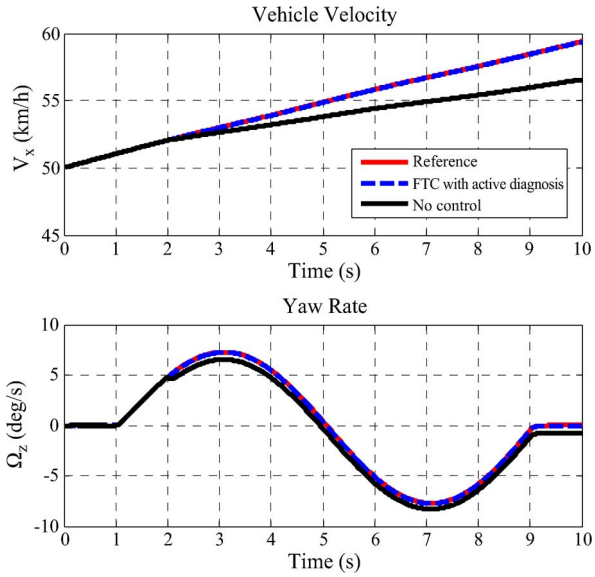

Fig. 12. Longitudinal velocities and yaw rates in single lane change.

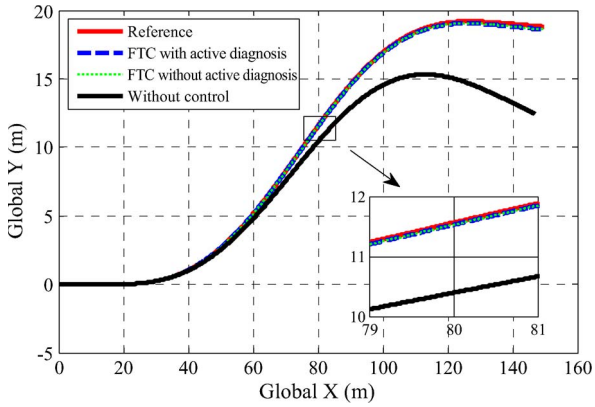

Fig. 13. Vehicle trajectories in single lane change.

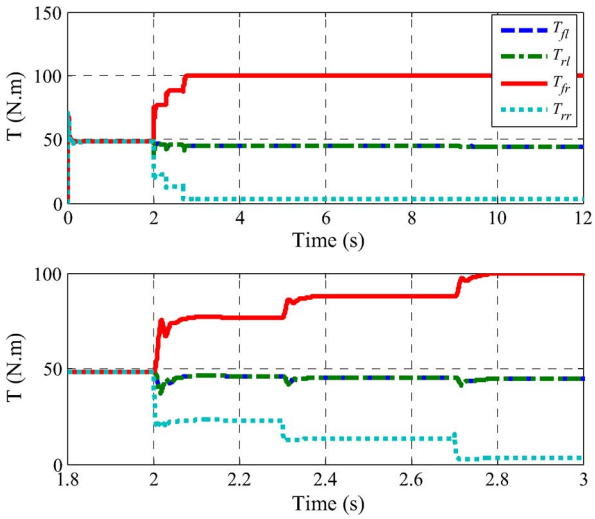

Fig. 14. Motor torques in the split-μ test (controlled by FTC with active fault diagnosis).

the vehicle well. Note that the FTC with active fault diagnosis can reallocate the control efforts based on the diagnosis result. Fig. 17 also shows that the controlled vehicles cannot

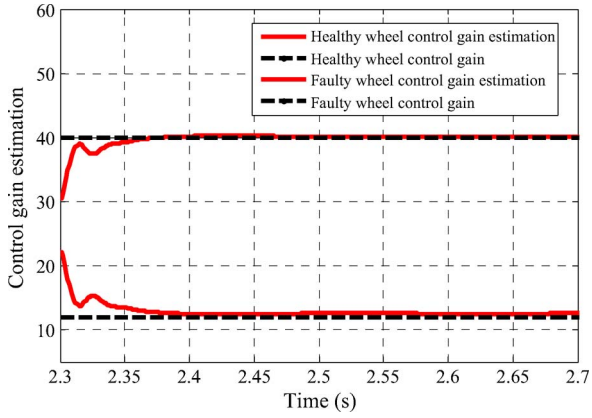

Fig. 15. Control gain estimations of the two wheels on the faulty side in the split-μ simulation.

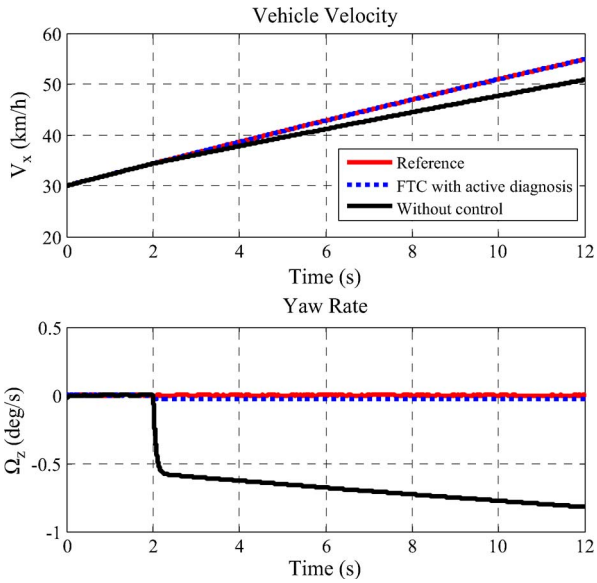

Fig. 16. Longitudinal velocities and yaw rates in split-μ simulation.

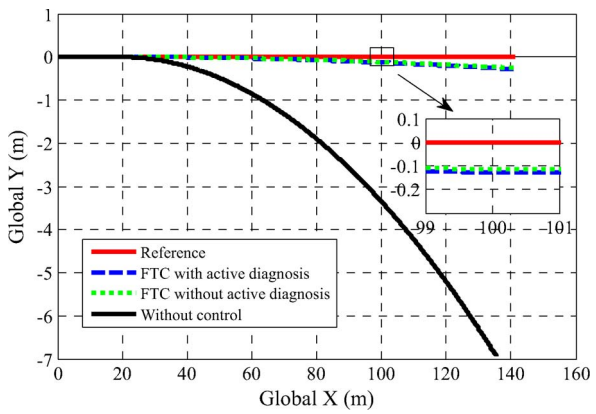

Fig. 17. Vehicle trajectories in the split-μ simulation.

exactly follow the reference trajectory. This is because that even through the yaw rate following error is very small, as shown in the simulation results, the error accumulation will still make the yaw angle deviate from the desired value a little and, consequently, results in some vehicle trajectory tracking error.

Note that in this paper, the situation of road frictional coefficient sudden change is not considered. How to differentiate the road frictional condition sudden change and motor fault may deserve another further investigation. In addition, as indicated in the previous section, the method is independent of the faulty wheel location.

VI. Conclusion

A fault-tolerant control approach for a 4WID electric vehicle with in-wheel motors has been proposed in this paper. An adaptive FTC is employed to maintain the vehicle stability and desired motions when an in-wheel motor/motor driver fault happens and when the active fault diagnosis is being conducted. For addressing the challenges of fault isolation for overactuated systems, an active fault diagnosis method is designed to explicitly isolate the faulty motor and evaluate the motor fault under passive FTC. Despite the small motor control gain estimation errors caused by model inaccuracies, the active fault diagnosis and control gain estimation can provide sufficient information for redistributing the control efforts among the wheels to discourage the use of the faulty wheel motor for avoiding further damages. Simulations using a high-fidelity CarSim full-vehicle model show the effectiveness of the proposed active fault diagnosis and fault-tolerant control approaches in various driving conditions.

References

[1] C. C. Chan, "The state of the art of electric and hybrid vehicles," *Proc. IEEE*, vol. 95, no. 4, pp. 704–718, Apr. 2007.

[2] J. Yamakawa, A. Kojimaa, and K. Watanabe, "A method of torque control for independent wheel drive vehicles on rough terrain," *J. Terramech.*, vol. 44, no. 5, pp. 371–381, Nov. 2007.

[3] M. Shino and M. Nagai, "Independent wheel torque control of small-scale electric vehicle for handling and stability improvement," *JSAE Rev.*, vol. 24, no. 4, pp. 449–456, Oct. 2003.

[4] Y. Chen and J. Wang, "Adaptive vehicle speed control with input injections for longitudinal motion independent road frictional condition estimation," *IEEE Trans. Veh. Technol.*, vol. 60, no. 3, pp. 839–848, Mar. 2011.

[5] R. Wang and J. Wang, "Fault-tolerant control for electric ground vehicles with independently-actuated in-wheel motors," *ASME Trans. J. Dyn. Syst. Meas. Control*, 2011, DOI: 10.1115/1.4005050, to be published.

[6] J. Wang and R. G. Longoria, "Coordinated and reconfigurable vehicle dynamics control," *IEEE Trans. Control Syst. Technol.*, vol. 17, no. 3, pp. 723–732, May 2009.

[7] W. Liang, H. Yu, R. McGee, M. Kuang, and J. Medanic, "Vehicle pure yaw moment control using differential tire slip," in *Proc. Amer. Control Conf.*, Jun. 2009, pp. 3331–3336.

[8] A. Sohel and L. Chen, "An analytical redundancy-based fault detection and isolation algorithm for a road-wheel control subsystem in a steer-by-wire system," *IEEE Trans. Veh. Technol.*, vol. 56, no. 5, pp. 2859–2869, Sep. 2007.

[9] R. Jayabalan and B. Fahimi, "Monitoring and fault diagnosis of multi-converter systems in hybrid electric vehicles," *IEEE Trans. Veh. Technol.*, vol. 55, no. 5, pp. 1475–1484, Sep. 2006.

[10] R. Isermann, R. Schwartz, and S. Stolzl, "Fault-tolerant drive-by-wire systems," *IEEE Control Syst. Mag.*, vol. 27, no. 5, pp. 64–81, Oct. 2002.

[11] J. Da Wu and C. Q. Chuang, "Fault diagnosis of internal combustion engines using visual dot patterns of acoustic and vibration signals," *NDT E Int.*, vol. 38, no. 8, pp. 605–614, Dec. 2005.

[12] M. Nyberg and T. Stutte, "Model based diagnosis of the air path of an automotive diesel engine," *Control Eng. Pract.*, vol. 12, no. 5, pp. 513–525, May 2004.

[13] N. Meskin and K. Khorasani, "Fault detection and isolation of actuator faults in overactuated systems," in *Proc. Amer. Control Conf.*, Jul. 11–13, 2007, pp. 2527–2532.

[14] H. Yang, V. Cocquempot, and B. Jiang, "Optimal fault-tolerant path-tracking control for 4WS4WD electric vehicles," *IEEE Trans. Intell. Transp. Syst.*, vol. 11, no. 1, pp. 237–243, Mar. 2010.

[15] H. Yang, V. Cocquempot, and B. Jiang, "Hybrid fault tolerant tracking control design for electric vehicles," in *Proc. 16th Mediterranean Conf. Control Autom.*, Jun. 25–27, 2008, pp. 1210–1215.

[16] O. Wallmark, L. Harnefors, and O. Carlson, "Control algorithms for a fault-tolerant PMSM drive," *IEEE Trans. Ind. Electron.*, vol. 54, no. 4, pp. 1973–1980, Aug. 2007.

[17] M. Muenchhof, M. Beck, and R. Isermann, "Fault-tolerant actuators and drives—Structures, fault detection principles and applications," *Annu. Rev. Control*, vol. 33, no. 2, pp. 136–148, Dec. 2009.

[18] S. Nandi, H. A. Toliyat, and X. Li, "Condition monitoring and fault diagnosis of electrical motors—A review," *IEEE Trans. Energy Convers.*, vol. 20, no. 4, pp. 719–729, Dec. 2005.

[19] I. Hwang, S. Kim, Y. Kim, and C. E. Seah, "A survey of fault detection, isolation, and reconfiguration methods," *IEEE Trans. Control Syst. Technol.*, vol. 18, no. 3, pp. 636–653, May 2010.

[20] H. K. Khalil, *Nonlinear Systems*. Englewood Cliffs, NJ: Prentice-Hall, 2002.

[21] G. Tao, *Adaptive Control Design and Analysis*. New York: Wiley, 2003.

[22] J. Y. Wong, *Theory of Ground Vehicles*, 3rd ed. New York: Wiley, 2001.

[23] H. B. Pacejka and E. Bakker, "The Magic Formula tire model," *Veh. Syst. Dyn.*, vol. 21, no. 1, pp. 1–18, 1992.

[24] S. Di Cairano and H. E. Tseng, "Driver-assist steering by active front steering and differential braking: design, implementation and experimental evaluation of a switched model predictive control approach," in *Proc. 49th IEEE Conf. Decis. Control*, Dec. 2010, pp. 2886–2891.

[25] H. B. Pacejka, *Tire and Vehicle Dynamics*, 2nd ed. Warrendale, PA: SAE Int., 2006.

[26] S. Sastry and M. Bodson, *Adaptive Control: Stability, Convergence and Robustness*. Englewood Cliffs, NJ: Prentice-Hall, 1989.

[27] R. Wang, Y. Chen, D. Feng, X. Huang, and J. Wang, "Development and performance characterization of an electric ground vehicle with independently actuated in-wheel motors," *J. Power Sources*, vol. 196, no. 8, pp. 3962–3971, Apr. 2011.

[28] S. Horiuchi, K. Okada, and S. Nohtomi, "Improvement of vehicle handling by nonlinear integrated control of four wheel steering and four wheel torque," *JSAE Rev.*, vol. 20, no. 4, pp. 459–464, Oct. 1999.

[29] R. Rajamani, D. Piyabongkarn, J. Y. Lew, and J. A. Grogg, "Algorithms for real-time estimation of individual wheel tire-road friction coefficients," in *Proc. Amer. Control Conf.*, Jun. 14–16, 2006, pp. 4682–4687.

[30] R. Rajamani, *Vehicle Dynamics and Control*. New York: Springer-Verlag, 2006.

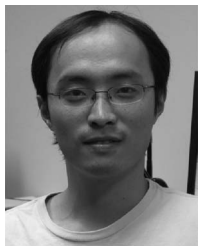

Rongrong Wang received the B.E. degree in control science and engineering from Tianjin University, Tianjin, China, in 2006, the B.S. degree in economics from Nankai University, Tianjin, in 2006, and the M.S. degree in control science and engineering from Tsinghua University, Beijing, China, in 2009. He is currently working toward the Ph.D. degree with the Vehicle Systems and Control Laboratory, Department of Mechanical and Aerospace Engineering, Ohio State University, Columbus.

His research interests include nonlinear systems control, fault-tolerant control, and vehicle dynamics and control.

Junmin Wang (M'06) received the B.E. degree in automotive engineering and the M.S. degree in power machinery and engineering from the Tsinghua University, Beijing, China, in 1997 and 2000, respectively, the M.S. degrees in both electrical engineering and mechanical engineering from the University of Minnesota, Twin Cities, in 2003, and the Ph.D. degree in mechanical engineering from the University of Texas at Austin, Austin, in 2007.

He has five years of full-time industrial research experience (May 2003–August 2008) with the Southwest Research Institute, San Antonio, TX. Since September 2008, he has been an Assistant Professor with the Department of Mechanical and Aerospace Engineering, The Ohio State University, Columbus. He is the author/coauthor of over 90 peer-reviewed papers on journals and conference proceedings and is the holder of 10 U.S. patents. His research interests include control, modeling, estimation, and diagnosis of dynamical systems, specifically for engine, powertrain, after treatment, hybrid, flexible fuel, alternative/renewable energy, (electric) ground vehicle, transportation, sustainable mobility, and mechatronic systems.

Dr. Wang is the Chair (2010–2012) of the SAE International Control and Calibration Committee and the Secretary (2010–2012) of the American Society of Mechanical Engineers (ASME) Automotive and Transportation Systems Technical Committee. He serves as an Associate Editor for the IEEE TRANSACTIONS ON VEHICULAR TECHNOLOGY, Conference Editorial Board of ASME Dynamic Systems and Control Division, American Control Conference, and ASME Dynamic Systems and Control Conference. He was the recipient of the Office of Naval Research Young Investigator Program (ONR-YIP) Award, the ORAU Ralph E. Powe Junior Faculty Enhancement Award in 2009, and one of the recipients of the 2009 SAE Vincent Bendix Automotive Electronics Engineering Award.